Remote Sensing of Environment 311 (2024) 114249

Contents lists available at ScienceDirect

Remote Sensing of Environment

journal homepage: www.elsevier.com/locate/rse

Estimation of boreal forest biomass from ICESat-2 data using hierarchical hybrid inference

Petri Varvia [a,*], Svetlana Saarela [b], Matti Maltamo [a], Petteri Packalen [c], Terje Gobakken [b], Erik Næsset [b], Göran Ståhl [d], Lauri Korhonen [a]

[a] School of Forest Sciences, University of Eastern Finland, P.O. Box 111, Joensuu, FI-80101, Finland
[b] Faculty of Environmental Sciences and Natural Resource Management, Norwegian University of Life Sciences, P.O. Box 5003, NMBU, Ås, NO-1432, Norway
[c] Natural Resources Institute Finland, Latokartanonkaari 9, Helsinki, FI-00790, Finland
[d] Faculty of Forest Sciences, Swedish University of Agricultural Sciences, SLU Skogsmarksgrand 17, Umeå, SE-90183, Sweden

ARTICLE INFO

Edited by Marie Weiss

Dataset link: https://doi.org/10.5281/zenodo.8083337

Keywords:
ICESat-2
Above-ground biomass
Boreal forest
Inference
Lidar

ABSTRACT

The ICESat-2, launched in 2018, carries the ATLAS instrument, which is a photon-counting spaceborne lidar that provides profile samples over the terrain. While primarily designed for snow and ice monitoring, there has been a great interest in using ICESat-2 to predict forest above-ground biomass density (AGBD). As ICESat-2 is on a polar orbit, it provides good spatial coverage of boreal forests.

The aim of this study is to evaluate the estimation of mean AGBD from ICESat-2 data using a hierarchical modeling approach combined with rigorous statistical inference. We propose a hierarchical hybrid inference approach for uncertainty quantification of the average AGBD of the area of interest estimated directly from a sample of ICESat-2 lidar profiles. Our approach models the errors coming from the multiple modeling steps, including the allometric models used for predicting tree-level AGB. For testing the procedure, we have data from two adjacent study sites, denoted Valtimo and Nurmes, of which Valtimo site is used for model training and Nurmes for validation.

The ICESat-2 estimated mean AGBD in the Nurmes validation area was 65.7 ± 1.9 Mg/ha (relative standard error of 2.9%). The local reference hierarchical model-based estimate obtained from wall-to-wall airborne lidar data was 63.9 ± 0.6 Mg/ha (relative standard error of 1.0%). The reference estimate was within the 95% confidence interval of the ICESat-2 hierarchical hybrid estimate. The small standard errors indicate that the proposed method is useful for AGBD assessment. However, some sources of error were not accounted for in the study and thus the real uncertainties are probably slightly larger than those reported.

1. Introduction

Satellite lidars have potential to improve the accuracy of global above-ground biomass (AGB) surveys by providing information on the forest height (Duncanson et al., 2019). Research into using spaceborne lidar data in AGB estimation started with the first ICESat mission (e.g. Lefsky et al., 2005; Boudreau et al., 2008; Nelson et al., 2017). ICESat has since been followed by GEDI, a dedicated forest observation mission on the International Space Station (Dubayah et al., 2020), and ICESat −2, launched in 2018 (Markus et al., 2017).

The ICESat −2 carries the ATLAS (Advanced Topographic Laser Altimeter System) instrument which is a profiling photon counting lidar operating at green wavelength (532 nm). ICESat −2 data consist of parallel ground tracks produced by the three pairs of strong and weak beams, which have a power ratio of 4:1 (Neumann et al., 2019). While primarily designed for snow and ice monitoring, ICESat −2 has the advantage of providing a good coverage of the boreal zone, the northern parts of which are not covered by GEDI.

The current spaceborne lidar sensors have a limitation that the measurements consist of either discrete footprints or, in the case of ICESat −2, discrete height profiles. As it is unlikely that the discrete footprints or profiles overlap with the ground sites with AGB field measurements, the construction of regression models that link AGB with the satellite measurements is more complicated than, for example, in optical satellite imagery provided as spatially continuous data. The current practice is to use airborne laser scanning (ALS) to bridge the gap between reference field measurements and the satellite measurements (e.g. Wulder et al., 2012), either by constructing an intermediate proxy model (e.g. Margolis et al., 2015; Holm et al., 2017; Narine

* Corresponding author.
E-mail address: petri.varvia@uef.fi (P. Varvia).

https://doi.org/10.1016/j.rse.2024.114249
Received 10 July 2023; Received in revised form 17 April 2024; Accepted 4 June 2024
Available online 10 June 2024

et al., 2020; Varvia et al., 2022; Guerra-Hernández et al., 2022) or by simulating satellite lidar measurements from the ALS data (Narine et al., 2019; Duncanson et al., 2022). It is also possible to measure field plots directly at the space lidar footprint or track locations (Lefsky et al., 2005; Nelson et al., 2009; Song et al., 2022), although in practice it is often not feasible due to e.g. poor accessibility of the footprint locations.

In addition to producing estimates of AGB or its areal density (AGBD), it is important to quantify the uncertainty of the estimated values, for example, by variance estimation. However, estimating the variance of the estimated AGB is complicated by the hierarchical modeling approach and the methodology has matured only relatively recently. As the response variables of the spaceborne lidar model are not coming from field measurements, but are predictions from the linking proxy model, they have an associated uncertainty. In the earliest studies, such as Nelson et al. (2009), the uncertainty from this model hierarchy was omitted due to intractability.

The first study to account for multiple modeling steps in space lidar application was Holm et al. (2017), which used the so-called hybrid inference approach (Ståhl et al., 2011) and reformulation of the hierarchical modeling to a more tractable form to include the uncertainty from the proxy ALS model. In hybrid inference, the model predictions at the satellite lidar footprint or track level are treated in a similar way as observations in traditional design-based inference, such as measured sample plots in a forest inventory. As the observations are model predictions with associated uncertainty, a hybrid estimate combines the variance coming from the sample design with the propagated variance coming from model uncertainty. Hybrid inference has been used in several previous space lidar studies (e.g. Healey et al., 2012; Neigh et al., 2013; Margolis et al., 2015; Nelson et al., 2017; Patterson et al., 2019). However, there is still a need for further development and evaluation of variance estimation for multiple modeling steps. For example in the case of AGB estimation, the field plot biomass values are not direct measurements, but predictions from allometric models based on e.g. measured stem diameters and tree heights, which has not been assessed in previous space lidar studies.

A parallel development to variance estimation in the case of hierarchical modeling was the so-called hierarchical model-based (HMB) approach (Saarela et al., 2016, 2020), which was originally applied to a scenario where a proxy ALS model is used to link field plot data to wall-to-wall satellite imagery. HMB has since been applied also to satellite lidar applications, such as GEDI (Saarela et al., 2018, 2022).

The aim of this study is to evaluate the estimation of the mean AGBD and its variance using a hierarchical modeling procedure with ICESat −2, Sentinel-2, ALS and field data. We propose a hierarchical hybrid inference approach that combines error propagation through the model hierarchy in HMB with the hybrid inference approach (Saarela et al., 2023). The hybrid estimation approach is conceptually similar to what has been previously done with GEDI data (e.g. Patterson et al., 2019; Dubayah et al., 2022), but instead of simulating ICESat −2 measurements, a proxy model based on ALS and Sentinel-2 data is used to connect ICESat −2 data to field-measured AGBD. We also include the uncertainty of the allometric models used to produce field-plot AGBD values, which has been omitted in previous space lidar studies. The uncertainty of these modeling steps is propagated similar to HMB. To the authors' knowledge, this is the first study where hybrid inference is used with ICESat −2 data. It is also the first time hierarchical hybrid inference with three modeling phases (allometry, ALS, and spaceborne lidar) is tested with real remote sensing data.

2. Materials

2.1. Study sites and field measurements

The two adjacent study areas are located near Valtimo (N 63°46′ E 28°13′) and Nurmes, Finland (N 63°46′ E 29°37′). (Fig. 1) Both consist of similar boreal forests, dominated by Scots pine (*Pinus sylvestris* L.), with a minority of Norway spruce (*Picea abies* (L.) Karst) and birches (*Betula* spp.). The Valtimo site is approximately 60 × 50 km in size and the Nurmes site is 50 × 50 km. We used sample plots measured by the Finnish Forest Centre as a part of ALS-based forest management inventories in the summers 2019 and 2020 in Valtimo and Nurmes, respectively.

Table 1
Summary of the field plot data. Height is the plot average. SD is standard deviation. The minimum values of zero represent plots with no trees with DBH ≥ 5 cm.

	Mean	SD	Min	Max
Valtimo				
Height [m]	10.2	5.5	0	25.0
DBH [cm]	10.9	6.3	0	35.0
AGBD [Mg/ha]	62.6	49.5	0	298.8
Nurmes				
Height [m]	10.7	5.4	0	23.8
DBH [cm]	11.9	6.7	0	31.8
AGBD [Mg/ha]	66.5	57.4	0	282.8

The Valtimo site was used to train an ICESat −2 prediction model, which was then applied to obtain AGBD predictions for the bordering Nurmes site. Both sites had their own field, airborne, and spaceborne data sets that were obtained in different years. Thus we could evaluate ICESat −2 prediction accuracy and uncertainty estimation in the Nurmes site independently of Valtimo, but without confounding effects from geographic variation.

The field data included circular plots with radius of either 5.64 m, 9.00 m, or 12.62 m depending on the forest maturity. In total, there are 797 field plots in the Valtimo area (24 $r = 5.64$ m, 839 $r = 9$ m, and 80 $r = 12.62$ m) and 891 plots in the Nurmes area (212 $r = 5.64$ m, 489 $r = 9$ m, and 190 $r = 12.62$ m). At each plot, diameter at breast height (DBH) was measured for each tree with DBH ≥ 5 cm. The height of a sample tree of each species was measured on each plot and a mixed-effect height model was calibrated to the local area using the sample trees (Eerikäinen, 2009) and used to predict the height for the rest of the trees. A summary of the field-plot data is presented in Table 1.

2.2. ALS data

The ALS data in the Valtimo area were collected between June 7th and July 9th 2019 using a Leica ALS 80 HP scanner. The flying altitude was 1700 m above ground level, resulting in a nominal pulse density of 5 p/m^2 and a footprint diameter of 39 cm. In the Valtimo area, the publicly available data were used, which were resampled from 5 p/m^2 to 0.5 p/m^2 before distribution. While the resampled data had a low pulse density, it was sufficient for area-based approach (e.g. Maltamo et al., 2006; Wilkes et al., 2015). The ALS data in the Nurmes area were collected between June 17th and June 22nd 2020 using a Riegl VQ-1560i scanner at a flying altitude of 2100 m. In the Nurmes area the original point cloud with > 5 p/m^2 was used.

The ALS processing was done identically for both sites. The ALS echoes were height normalized with respect to ground using LAStools (Isenburg, 2020). For each plot, canopy metrics were computed using "first-of-many" plus "only" echoes, and "last-of-many" plus "only" echoes, producing two sets of metrics. The metrics included mean and maximum heights, standard deviation of heights, height percentiles $p_5, p_{10}, p_{20}, \ldots, p_{90}, p_{95}, p_{99}$, canopy density percentiles (bincentiles) $b_5, b_{10}, b_{20}, \ldots, b_{90}, b_{95}$, canopy cover, and the mean and standard deviation of intensities. The canopy density percentiles (bincentiles) were calculated as the percentage of echoes between the height cutoff (here 0 m) and a percentage of the maximum height, i.e. b_{90} is the number of echoes with height between zero and 90% of the maximum divided by the total number of echoes expressed in percents. Canopy cover was calculated as the fraction of echoes with height above 2 m.

Fig. 1. Location of the study sites Valtimo (N 63°46′ E 28°13′) and Nurmes (N 63°46′ E 29°37′) in Finland.

2.3. Sentinel-2 data

For the Valtimo site, a cloud-free Sentinel-2 image was available from June 14th 2019. For the Nurmes site, a cloud-free Sentinel-2 composite was constructed from images captured on June 16th, July 16th, and July 18th 2020. Atmospheric correction of the Sentinel-2 images was done using Sen2Cor (Main-Knorn et al., 2017), after which the atmospheric bands (bands 1, 9, and 10) were omitted. The images were then calibrated using histogram matching before compositing. The pixel values were used as predictors in the proxy AGBD models, in addition to several common spectral vegetation indices calculated from the images.

2.4. ICESat −2 data

The ATL03 (Neumann et al., 2021) and ATL08 (Neuenschwander et al., 2021) data for the Valtimo site covered the period from October 2018 to December 2019. For the Nurmes site, ATL03 and ATL08 data captured during the year 2020 were used. Version 4 of the data products were used for both sites.

The ICESat −2 data were processed following Varvia et al. (2022). First, the ICESat −2 tracks were split into 90 m × 15 m segments, centered on the locations of the ATL08 product. Each 90 m segment was further divided into six 15 m × 15 m subcells, which were used for the prediction of proxy AGBD on the 90 m track segments. The ATL08 individual photon classifications were then matched with the photon locations from ATL03 product. Photons classified as noise were discarded. The segment length of 90 m was chosen to ensure that there are enough signal photons (e.g. more than 100) to reduce random variability in the height metrics due to limited number of photons.

The classified photons were then clipped to the 90 m track segments. Using the photons classified as ground, the above-ground height was computed for each photon using LAStools by subtracting a triangular irregular network representing ground photons from the raw photon heights. Several height metrics were then calculated, and similar to the ALS metrics detailed above, they included the number of photons (canopy only (n_c) and total (n_{all})), mean photon height, standard deviation, maximum, height percentiles $p_5, p_{10}, p_{20}, \ldots, p_{90}, p_{95}, p_{99}$, canopy density percentiles $b_5, b_{10}, b_{20}, \ldots, b_{90}, b_{95}$, and mean square height (qav). As with ALS data, height cutoff of 0 m was used. The mean square height is the average of the squared photon heights.

Poor quality segments were omitted if they did not meet the criteria of at least 100 classified photons and a fraction of high confidence photons (`signal_conf_ph` in ATL03) being at least 60%. In addition, a polygonal forest mask produced by the Finnish Forest Centre (Finnish Forest Centre, 2021) was used to discard ICESat −2 segments in certain non-forested areas, such as agricultural fields, water, roads, and built-up areas.

We used only strong beam data captured outside the snowy season during daytime. While night data would be preferable due to the absence of solar noise, not enough snowless strong beam night data were available from the Nurmes site (only 60 segments). The use of daytime data thus represents a compromise between expected performance and data availability. For the Valtimo area there was a total of 1721 valid 90 m segments and 5760 segments in Nurmes (Fig. 2). The areal sampling fraction (area of the ICESat −2 90 m segments divided by the total forested area) was 0.3% in the Nurmes area.

3. Methods

The process of estimating AGBD using ICESat −2 data follows hierarchical modeling with three steps: (1) deriving field-plot AGBD from allometric AGB models and measured trees, (2) model based on ALS and Sentinel-2 data for predicting proxy AGBD on ICESat −2 tracks, and (3) ICESat −2 model for predicting AGBD from ICESat −2 height metrics. The model chain is trained using the data from Valtimo area and the fitted ICESat −2 model is then used to predict AGBD with the Nurmes data.

We used the species-specific biomass models by Repola (2008, 2009) to predict allometric AGB for each measured tree on the field plots using the calipered DBH and predicted tree height. The field-plot AGBD was then calculated by summing up the tree-level AGBs of each plot and scaled to per-hectare level A.1. The covariance matrix of the tree-level AGBs was calculated using the estimated covariances of the species-specific biomass model parameters reported in Ståhl et al. (2014). The tree-level covariances were then aggregated to derive covariance matrix for the plot-level AGBDs.

A quadratic model with four variables was then fitted between the field-plot AGBD, and ALS and Sentinel-2 metrics using generalized nonlinear least squares. The four metrics in the model were chosen using a simulated annealing based variable selection routine (Packalen et al., 2012) from the ALS and Sentinel-2 metrics without constraints on the number of included Sentinel-2 variables. The ALS and Sentinel-2 model was then used to predict proxy AGBD on the 15 m × 15 m subcells constructed on the ICESat −2 tracks. The subcell AGBDs were averaged to calculate proxy AGBD values for the 90 m track segments used in the ICESat −2 modeling A.2. Covariance matrix for the 15 m subcell AGBDs was derived using HMB (Saarela et al., 2020) by including both the uncertainty of the fitted ALS and Sentinel-2 model parameters and the covariance matrix for the plot-level AGBDs stemming from the allometric models. The 15 m subcell AGBD covariances were then aggregated to produce a covariance matrix for the 90 m proxy AGBDs.

In the final modeling step, a quadratic model with four variables was fitted between the 90 m proxy AGBD and ICESat −2 metrics; the four metrics were again chosen using simulated annealing. This model was then used to predict AGBD on the Nurmes ICESat −2 track

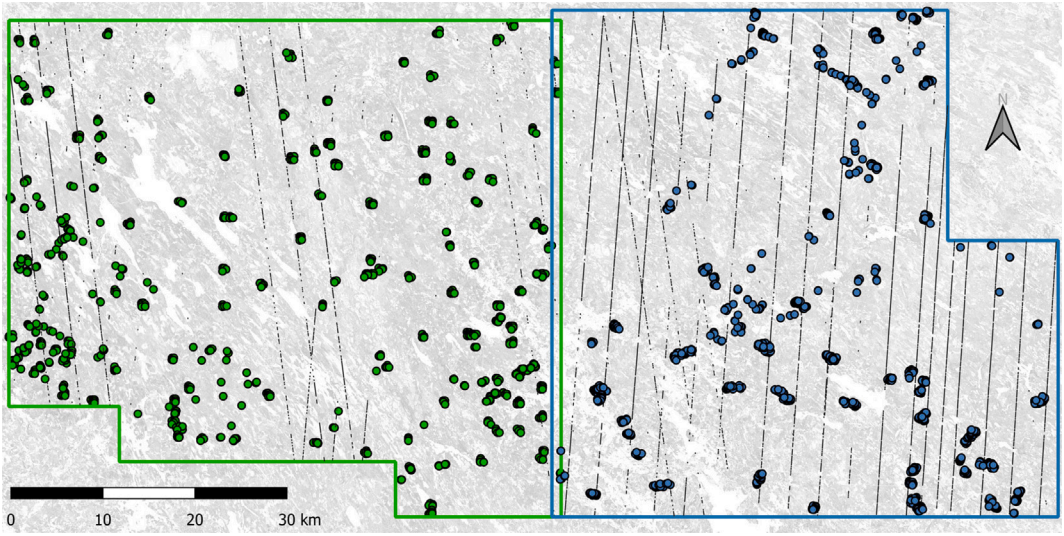

Fig. 2. The locations of 90 m ICESat −2 segments in Valtimo (left, green) and Nurmes (right, blue) superimposed on a canopy height map (Finnish Forest Centre). Field plot locations shown with circles. (For interpretation of the references to color in this figure legend, the reader is referred to the web version of this article.)

segments A.3. As with the previous model step, the covariance matrix of the ICESat −2 AGBD predictions was estimated using HMB by including the uncertainty of the fitted ICESat −2 model parameters and the covariance matrix of the 90 m proxy AGBDs.

The AGBD predictions on the Nurmes ICESat −2 track segments were used to calculate a hierarchical hybrid estimate for the mean and variance of AGBD in the Nurmes area. The predictions on the track segments were modeled as a clustered random sample (Ståhl et al., 2011), where each ICESat −2 track was a cluster, similar to what was previously done by Dubayah et al. (2022) with GEDI data. As the tracks can cross and overlap, the design is considered as sampling with replacement. For example, there were 18 overlapping segments in the Nurmes area. The estimate for mean AGBD is

$$\hat{\mu}_{\mathrm{I2}} = \frac{\sum_{i=1}^{n_{\mathrm{track}}} \widehat{\mathrm{AGBD}}_{\mathrm{I2,sum}}^{(i)}}{\sum_{i=1}^{n_{\mathrm{track}}} n_{\mathrm{seg}}^{(i)}}, \tag{1}$$

where $\widehat{\mathrm{AGBD}}_{\mathrm{I2,sum}}^{(i)}$ is the summed up predicted AGBD of the i'th ICESat −2 track, $n_{\mathrm{seg}}^{(i)}$ is the number of 90 m segments in the i'th track, and n_{track} is the number of tracks.

The hybrid estimator for AGBD variance consists of two parts. First is the design-based sampling variability under the assumed design

$$\widehat{\mathrm{Var}}_D(\hat{\mu}_{\mathrm{I2}}) = \frac{1}{\bar{n}_{\mathrm{seg}}^2} \frac{\sum_{i=1}^{n_{\mathrm{track}}} (\widehat{\mathrm{AGBD}}_{\mathrm{I2,sum}}^{(i)} - \hat{\mu}_{AGBD} n_{\mathrm{seg}}^{(i)})^2}{n_{\mathrm{track}}(n_{\mathrm{track}} - 1)}, \tag{2}$$

where $\bar{n}_{\mathrm{seg}}$ is the average number of segments per track. The second part is the model-based uncertainty of the predicted AGBDs, which is

$$\widehat{\mathrm{Var}}_M(\hat{\mu}_{\mathrm{I2}}) = \frac{1}{n_{\mathrm{tot}}^2} \mathbf{1}^T \hat{\mathbf{C}}_{\mathrm{I2}} \mathbf{1}, \tag{3}$$

where n_{tot} is the total number of ICESat −2 segments and $\mathbf{1}$ is a vector of ones. The covariance matrix $\hat{\mathbf{C}}_{\mathrm{I2}}$ is the hierarchical model-based covariance of the ICESat −2 predictions. For the derivation of $\hat{\mathbf{C}}_{\mathrm{I2}}$, see Appendix. Schematic of the error propagation in the model-based part is shown in Fig. 3. Finally, the estimated variance of the mean AGBD is

$$\widehat{\mathrm{Var}}(\hat{\mu}_{\mathrm{I2}}) = \widehat{\mathrm{Var}}_D(\hat{\mu}_{\mathrm{I2}}) + \widehat{\mathrm{Var}}_M(\hat{\mu}_{\mathrm{I2}}). \tag{4}$$

Additional details and derivation of the hierarchical hybrid approach are presented in the companion article by Saarela et al. (2023).

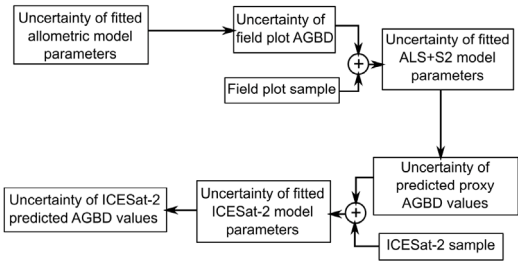

Fig. 3. Schematic of the error propagation.

3.1. Reference estimate

Hierarchical model-based (HMB) estimate calculated using an independent local data set was used as a reference estimate of mean AGBD at the Nurmes validation area (see Appendix A.4). As in the ICESat −2 workflow, a quadratic model with four variables was fitted between the field-plot AGBD, and ALS and Sentinel-2 metrics in Nurmes. The model was then used to produce a 15 m × 15 m wall-to-wall AGBD raster over the area. The variance estimation procedure followed Saarela et al. (2020) and included the uncertainty from the allometric models and the ALS and Sentinel-2 model fitted using the Nurmes field plots.

In addition to comparing the estimated mean AGBD and its variance, ICESat −2 model performance was evaluated using root mean square deviation (RMSD) (5) and mean difference (MD) (6). The ICESat −2 predictions in the Nurmes area were compared to AGBD predicted on the ICESat −2 segment locations using the local ALS and Sentinel-2 model.

$$\mathrm{RMSD} = \sqrt{\frac{1}{n} \sum \left(\widehat{\mathrm{AGBD}}_{\mathrm{I2}} - \widehat{\mathrm{AGBD}}_{\mathrm{proxy}} \right)^2} \tag{5}$$

$$\mathrm{MD} = \frac{1}{n} \sum \left(\widehat{\mathrm{AGBD}}_{\mathrm{I2}} - \widehat{\mathrm{AGBD}}_{\mathrm{proxy}} \right) \tag{6}$$

4. Results

4.1. AGBD models

The ALS and Sentinel-2 AGBD models and the ICESat −2 AGBD had a similar quadratic form with four predictors chosen using a simulated

annealing. The fitted ALS and Sentinel-2 proxy AGBD model in the Valtimo area was:

$$\widehat{\mathrm{AGBD}}_{\mathrm{proxy}} = (8.52 + 0.44\ \mathrm{avg}_f + 0.34\ \mathrm{avg}_l - 0.0013\ \mathrm{NIR} - 0.0012\ \mathrm{SWIR1})^2, \quad (7)$$

where avg_f is the average above-ground height of the ALS echoes that were either the only returned echo or the first of many echoes for a given laser pulse, avg_l is the average height of echoes that were either the only returned echo or the last of many echoes, NIR and SWIR1 are the Sentinel-2 NIR and SWIR1 channel values, respectively. The model was fitted using generalized nonlinear least squares (Pinheiro et al., 2021), with an estimated residual variance function of a constant plus power structure

$$\widehat{\mathrm{Var}}(\mathbf{e}_f) = 0.61^2 \left(6.23 + \widehat{\mathrm{AGBD}}_{\mathrm{proxy}}^{0.69}\right)^2. \quad (8)$$

Similarly, the ALS and Sentinel-2 model for the Nurmes validation area, which was used to obtain the reference HMB estimate, was

$$\widehat{\mathrm{AGBD}}_{\mathrm{ref}} = (9.77 - 0.034 b_{10,f} + 0.40 p_{99,l} - 0.042 b_{40,l} - 0.0012\ \mathrm{NIR})^2, \quad (9)$$

where $b_{10,f}$ is the 10th bincentile computed from the first-of-many and only echoes, $p_{99,l}$ is the 99th height percentile of last-of-many and only echoes, $b_{40,l}$ is the 40th bincentile of last-of-many and only echoes, and NIR is the Sentinel-2 NIR channel value. The fitted residual variance function was

$$\widehat{\mathrm{Var}}(\mathbf{e}_{\mathrm{ref}}) = 0.99^2 \left(2.78 + \widehat{\mathrm{AGBD}}_{\mathrm{ref}}^{0.61}\right)^2. \quad (10)$$

The simulated annealing variable selection was run separately for the Nurmes model to improve independence of the reference estimate and because the Nurmes ALS data had a different point density.

The proxy model (7) was applied to predict AGBD for the ICESat −2 segments at the Valtimo study area. These predictions were used as response AGBDs in the fitting of the ICESat −2 AGBD model in the Valtimo area:

$$\widehat{\mathrm{AGBD}}_{\mathrm{I2}} = (1.90 + 1.37\ \mathrm{std} + 0.12\sqrt{n_c} + 0.25\sqrt{p_{40}} - 0.61\sqrt{p_{80}})^2, \quad (11)$$

where std is the standard deviation of photon heights, n_c is the number of canopy photons, and p_{40} and p_{80} are the 40th and 80th canopy height percentiles, respectively. Residual variance was homoscedastic for the ICESat −2 model: $\widehat{\mathrm{Var}}(\mathbf{e}_g) = 433.0\ \mathrm{Mg}^2/\mathrm{ha}^2$.

Scatter density plots of the fitted models are shown in Fig. 4. The residual plots on the right side of Fig. 4 show the absolute residuals and the standard deviation of the fitted residual variance functions.

The ICESat −2 AGBD model (11) was then applied to predict the AGBD for the ICESat −2 segments in the Nurmes validation area. The accuracy of these predictions was first compared with the predictions obtained with the local ALS and Sentinel-2 model (9) at the Nurmes track locations. The ICESat −2 predictions had an RMSD of 21.3 Mg/ha (30.8%) and an MD of −3.3 Mg/ha (−4.8%). Scatter plot of the predictions is shown in Fig. 5. Summary of the training proxy AGBD and ICESat −2 model predictions in the Valtimo area, Nurmes area, and of the local ALS and Sentinel-2 model predictions are shown in Table 2. Histograms of the proxy AGBD and ICESat −2 predictions are shown in Fig. 6.

The 15 m resolution AGBD map produced using the local model based on ALS and Sentinel-2 data is shown in Fig. 7. Non-forested areas were discarded. Visible features are the Hiidenportti National Park and other protected forests in the north of the area, which are visible as yellow areas of large biomass values in the map. The area also has many open mires, which show up as blue areas of small AGBD.

Table 2
Statistical summaries of the estimated AGBD values at 90 m ICESat-2 track segment level. Units are Mg/ha.

Data	Min.	Q1	Median	Mean	Q3	Max
Train						
Valtimo, local ALS+S2	0	17.4	42.7	46.0	64.9	199.8
Valtimo, ICESat-2	5.9	23.0	43.9	45.8	62.7	174.0
Test						
Nurmes, local ALS+S2	0	37.9	67.3	69.0	94.9	278.3
Nurmes, ICESat-2	5.9	42.8	63.3	65.7	85.3	231.3

4.2. Variance estimation

The mean AGBD and its standard error over the forested parts of the Nurmes area was 65.7 ± 1.9 Mg/ha when using ICESat −2 data and hierarchical hybrid estimation (Table 3). The reference hierarchical model-based estimate using local ALS and Sentinel-2 data was 63.9±0.6 Mg/ha. The relative standard errors were 2.9% and 1.0%, respectively.

Summary of the model chain is shown in Fig. 8 with the contribution of the modeling steps to the total standard error (1.91 Mg/ha). The contributions were calculated by progressively removing error components and computing the resulting standard error. For example, to derive the contribution of the allometric model (0.04 Mg/ha), the total standard error was calculated by omitting the latter part of Eq. (A.7) which propagates the allometric model uncertainty. That is, the total standard error without allometric contribution (1.87 Mg/ha) was calculated by setting

$$\hat{\mathbf{C}}_{\boldsymbol{\beta}} = (\mathbf{J}_f^T \hat{\boldsymbol{\Sigma}}_f^{-1} \mathbf{J}_f)^{-1}, \quad (12)$$

where $\hat{\mathbf{C}}_{\boldsymbol{\beta}}$ is the covariance of the ALS and Sentinel-2 AGBD model parameters, $\mathbf{J}_f$ is the Jacobian matrix of the model, and $\hat{\boldsymbol{\Sigma}}_f$ is the residual error variance matrix. Eq. (12) is the standard covariance matrix of the fitted model parameters in nonlinear least squares and assumes that the training data, i.e. plot-level AGBD, have no uncertainty. By calculating the difference between the standard error with (1.91 Mg/ha) and without allometry (1.87 Mg/ha)0, we arrived at 0.04 Mg/ha (2.1% of the total) for the allometric contribution.

The contribution of ALS and Sentinel-2 model uncertainty is calculated in a similar way. By omitting the latter part in Eq. (A.12) for the covariance matrix of ICESat −2 model parameters, we assume that the proxy AGBD values are accurate and thus we ignore the ALS and Sentinel-2 model uncertainty. The resulting standard error was 1.81 Mg/ha. By comparing this to the standard error 1.87 Mg/ha, which includes the proxy AGBD uncertainty, but not the allometric uncertainty, we derived the ALS and Sentinel-2 model contribution as 0.06 Mg/ha (2.9%).

Finally, the contribution of the ICESat −2 model uncertainty is calculated by removing the model-based part, Eq. (3), in the hierarchical hybrid estimate (4). That is, we calculate the standard error using only the design-based part in Eq. (2). The design-only standard error was 1.61 Mg/ha (84.3%). By calculating the difference between the design-only standard error and the standard error including ICESat −2 model uncertainty 1.81 Mg/ha, the contribution of ICESat −2 model was 0.20 Mg/ha (10.7%).

In summary, the sources of uncertainty in order of decreasing magnitude were: sample design (1.61 Mg/ha, 84.3%), ICESat −2 model (0.20 Mg/ha, 10.7%), proxy AGBD model (0.06 Mg/ha, 2.9%), and allometry (0.04 Mg/ha, 2.1%).

5. Discussion

The average AGBD estimated using the ICESat −2 model transferred from a nearby area (65.7 ± 1.9 Mg/ha) was close to the value produced using the local ALS and Sentinel model (63.9 ± 0.6 Mg/ha). The reference estimate is within the 95% confidence interval of the

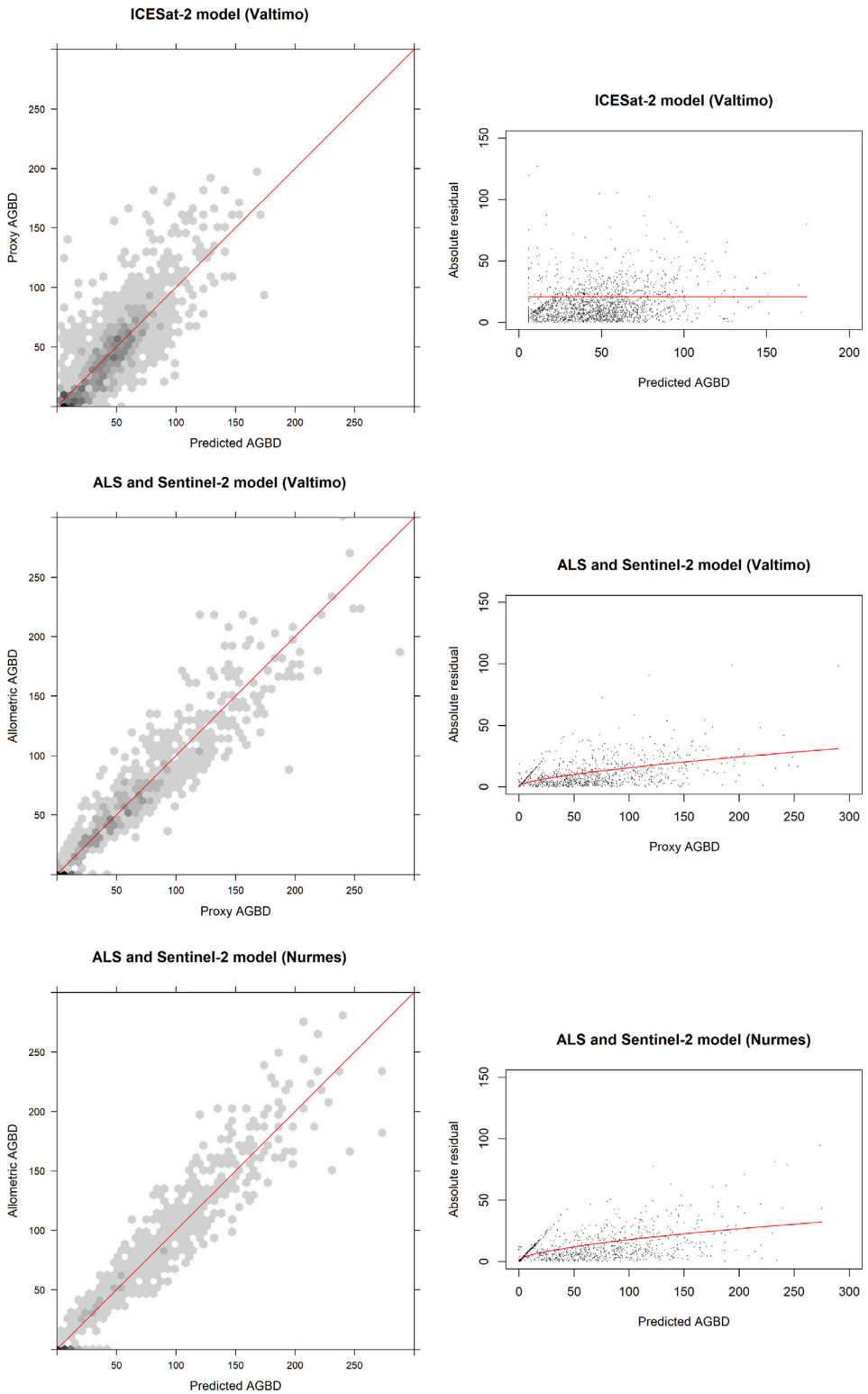

Fig. 4. Scatter density plots and absolute residuals of the fitted models. Red line in the residual plots shows the standard deviation from the residual variance model used in model fitting.

Table 3
Estimated average AGBD in the Nurmes area, its standard error and relative standard error for the hybrid hierarchical estimation using ICESat-2 and the reference hierarchical model-based estimate using local ALS and Sentinel-2 model.

Method	AGBD [Mg/ha]	Standard error [Mg/ha]	Relative standard error
Hierarchical hybrid	65.7	1.91	2.9%
Reference HMB	63.9	0.64	1.0%

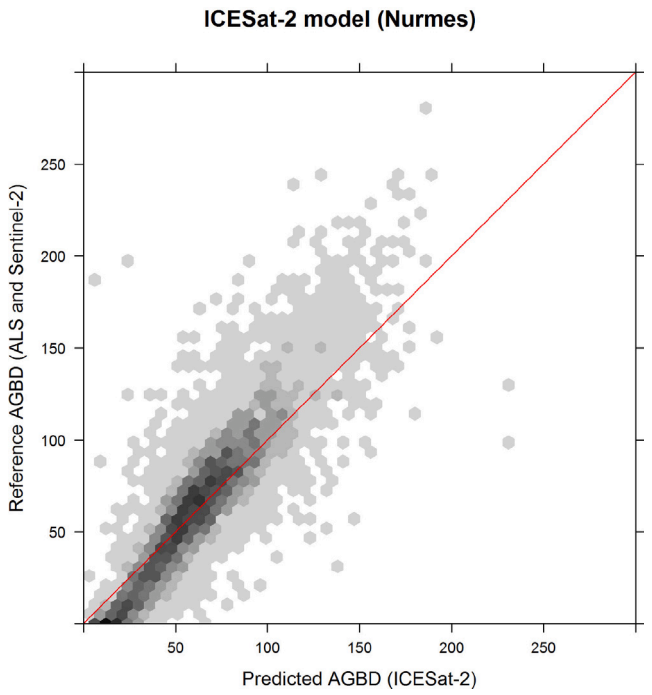

Fig. 5. A comparison of AGBDs predicted by the local ALS and Sentinel-2 model vs. the ICESat −2 model fitted in Valtimo training area for the Nurmes validation area.

ICESat −2 estimate. However, the comparison of ICESat −2 and reference model predictions at the track segment level revealed that the ICESat −2 model had a tendency to underestimate AGBD (MD of −3.3 Mg/ha). If the estimated MD was subtracted from the ICESat −2 model predictions, the average AGBD estimate would rise to 69.0 Mg/ha. In this case, the difference to the reference estimate would be 5.1 Mg/ha. Considering that the ICESat −2 model was transferred from adjacent area and previous year, this is still a promising result.

One reason for the observed systematic error in ICESat −2 AGBD predictions was that the ICESat −2 training data from the Valtimo area have smaller AGBD values (Table 2) than the Nurmes target population, on average by 23 Mg/ha. If the estimation process was scaled up, to e.g. country level, the problem could likely be mitigated by using more training data from a larger number of locations which would better capture the full variation in the population.

The estimated relative standard error (3.5%) of hybrid estimation is small, especially considering the complex model chain and relatively poor accuracy of the ICESat −2 model. This is partly due to using variance as an uncertainty measure: variance corresponds to the variation of the estimate around the expected value of the estimate. As seen in Table 2 and Fig. 6, the ICESat −2 model generally predicted biomass values that have less variation, which then also reduced the variation in the estimated mean AGBD. This seems to be an inherent property of long model chains, where each modeling step further reduces the variation (Saarela et al., 2023). This effect can be directly seen when comparing the reference HMB standard error (0.6 Mg/ha) to the model-based part in the hierarchical hybrid estimate (0.3 Mg/ha). An underlying assumption in variance as a uncertainty measure is also that the model is approximately unbiased in the target population. Based on the observed MD of the ICESat −2 predictions, the assumption likely did not hold.

The fraction of forested area covered by the ICESat −2 segments (sampling fraction) was 0.3%, which is smaller than in e.g. the GEDI biomass product (c. 2%) (Saarela et al., 2022). While the sampling fraction in this study is still considerably larger than in traditional field-plot based forest inventories (e.g. Breidenbach et al., 2020), the sparse sampling can hinder small area estimation. Sampling fraction could be increased by including data from multiple years, although due to the off-nadir pointing cycle of the ATLAS sensor, approximately same locations will be imaged every 2 years (Markus et al., 2017).

Mean square error (MSE)[1] of the estimator would likely be a better uncertainty measure by aiming to model the discrepancy between the estimate and the true value and thus accommodate for systematic errors. However, deriving a MSE estimator for a complex model hierarchy appears to be currently intractable, for example, due to the problem of cross-correlation of the spatial autocorrelation effects at different modeling steps. Further complicating the situation, addition of spatial correlation effects can have a relatively small effect on the quantified uncertainty in some cases. For example in Fortin et al. (2022) it slightly reduced the uncertainty compared to using only variance.

In this study, predicted tree heights were used in the allometric models due to unavailability of measured tree heights for all trees. This is a source of uncertainty that was omitted in the study, as it would add a further, complicating modeling step. Propagating the uncertainty from the estimated tree heights would likely require refitting of the mixed-effect models presented in Eerikäinen (2009).

Interpretation of the contribution of the model components to the resulting standard error (Fig. 8) is complicated by two factors. First is the decrease in variation described earlier. In addition to the modeling steps, the averaging of 15 m proxy AGBDs to the 90 m segments used in the ICESat −2 model further decreases the variation coming from allometry and the ALS and Sentinel-2 model. The second factor is a problem in calculating the contributions. Previously, Saarela et al. (2020) used fraction of the total variance to evaluate component contributions. We opted here to evaluate contribution using standard error by removing modeling steps one at a time and calculating the differences, primarily since standard error is in the same units as the estimate (Mg/ha) and thus could be easier to interpret. Both approaches have the limitation that the contribution of the lower modeling steps in the hierarchy cannot be evaluated directly, as they are affected by the propagation through the model chain. However, keeping these limitations in mind, the contribution of the model components to the total standard error is logical. The largest model-based contributor is the ICESat −2 model (10.7%), which is also the least accurate model when measured by goodness of fit. The order of the contributions of allometry and ALS and Sentinel-2 model are also in line with their respective performance.

The field data used in this study was composed of circular plots with a radius of either 5.64 m, 9.00 m, or 12.62 m, depending on the forest maturity. The ALS and Sentinel-2 model trained on the field plots was then used to predict on 15 × 15 m cells, which is closest in area to the 9.00 m radius plots, which are the most common type in the data. Based on the findings by Packalen et al. (2019), the 5.64 m and 12.62 m field plots can introduce a small bias (< 1%) in the proxy AGBD model when used to predict on the 15 m cells. The effect is likely negligible when propagated to the final standard error estimate.

The reference HMB estimate had a considerably smaller relative standard error (1.0%) compared to that reported by Saarela et al. (2020) (7.5%). The discrepancy seems to be mostly explained by differences in the data. The current study had a larger number of field plots, and Sentinel-2 data was used in addition to ALS, which resulted in a better performing AGBD model. The smaller positioning error of sample plots in this study (nominally < 1 meter) and the placement of field plots within the forest stands (never on stand borders) may also have contributed to the reference model accuracy. In the allometric modeling, Saarela et al. (2020) used separate models for trees with only measured diameter and for trees with measured diameter and height. We used models with measured diameter and estimated height for all trees. Comparatively small uncertainties in AGBD estimation have also been reported earlier by Esteban et al. (2019) (1.8%), although the study did not include allometric contribution.

[1] Not to be confused with the RMSD used previously to evaluate prediction accuracy, see e.g. Gregoire and Valentine (2007).

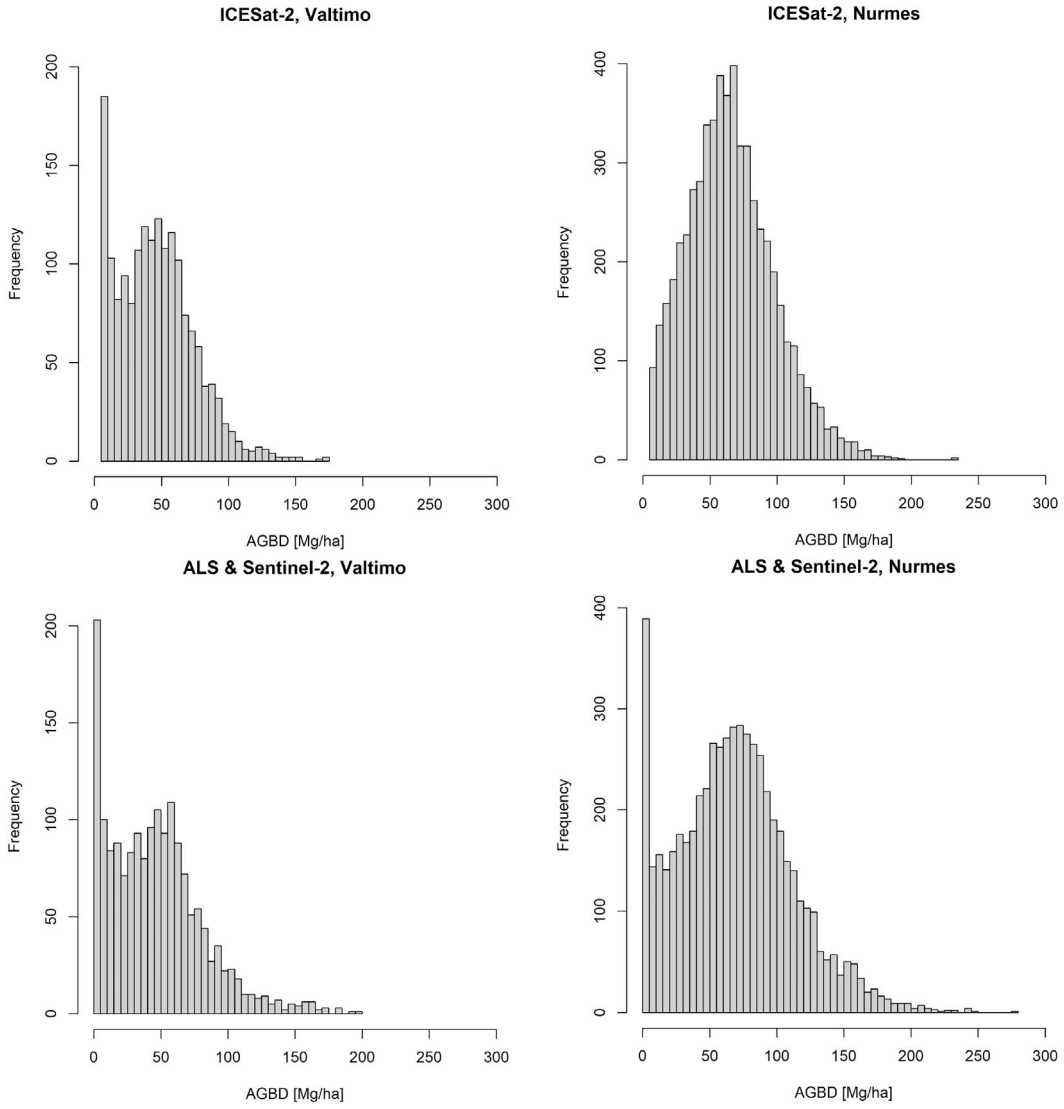

Fig. 6. Histograms of the ICESat −2 model predicted AGBD and the AGBD predicted by the local ALS and Sentinel-2 models in the Valtimo and Nurmes areas.

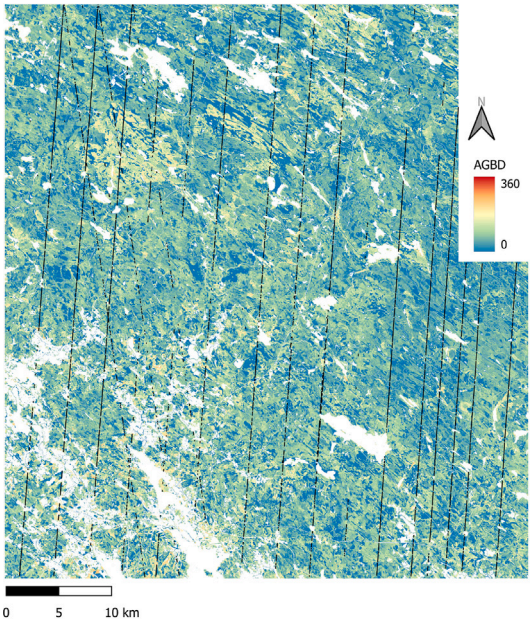

Fig. 7. 15 m resolution AGBD [Mg/ha] map of the Nurmes area produced using the reference ALS and Sentinel-2 model. ICESat −2 tracks shown in black.

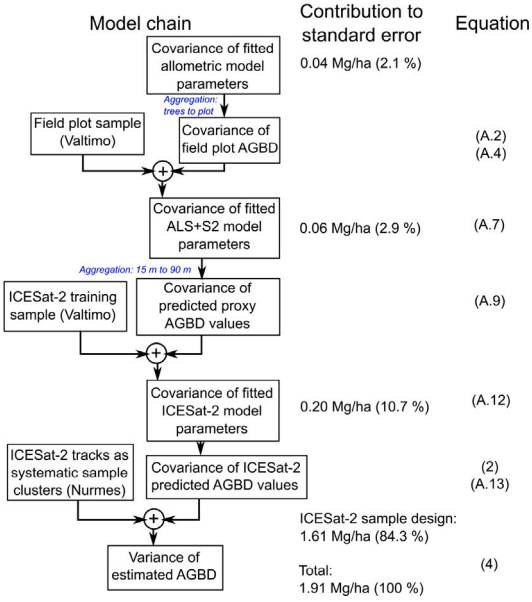

Fig. 8. Schematic of the model chain with contributions of the modeling steps to the final standard error. The corresponding equations in the Appendix and Section 3 are shown on right.

6. Conclusions

In this study, we evaluated estimation of average AGBD using ICESat −2 data and hierarchical modeling. Uncertainty of the estimated AGBD was quantified using hierarchical hybrid inference, which combines the error propagation through the multiple modeling steps with the variance coming from the sparse spatial coverage of the ICESat −2 data.

The ICESat −2 based estimate for the Nurmes validation area was 65.7 ± 1.9 Mg/ha compared to the local reference estimate of 63.9 ± 0.6 Mg/ha. The reference estimate was within the 95% confidence interval of the ICESat −2 based estimate. However, the interpretation was complicated by the observed presence of systematic error in the ICESat −2 AGBD predictions (−3.3 Mg/ha) at the validation area.

While the small estimated standard error should not be interpreted in the way that the proposed ICESat −2 estimate is highly reliable, the results support the use of ICESat −2 data for AGBD estimation. In this study, the ICESat −2 model was transferred from a different year and an adjacent area with relatively good results. Further studies should consider similar estimations for larger areas where also the structure of the forest can change.

CRediT authorship contribution statement

Petri Varvia: Writing – original draft, Software, Methodology, Investigation, Formal analysis, Data curation, Conceptualization. **Svetlana Saarela:** Writing – review & editing, Methodology, Formal analysis, Conceptualization. **Matti Maltamo:** Writing – review & editing, Conceptualization. **Petteri Packalen:** Writing – review & editing, Conceptualization. **Terje Gobakken:** Writing – review & editing, Methodology. **Erik Næsset:** Writing – review & editing, Methodology. **Göran Ståhl:** Writing – review & editing, Methodology. **Lauri Korhonen:** Writing – review & editing, Supervision, Project administration, Funding acquisition, Conceptualization.

Data availability

Data and codes area available at https://doi.org/10.5281/zenodo.8083337.

Acknowledgments

This study was supported by the Academy of Finland (grant numbers 332707 and 352782) and the Academy of Finland Flagship Programme (Forest-Human–Machine Interplay - Building Resilience, Redefining Value Networks and Enabling Meaningful Experiences (UNITE); grant numbers 357906 and 357909).

Declaration of competing interest

The authors declare that they have no known competing financial interests or personal relationships that could have appeared to influence the work reported in this paper.

Appendix. Error propagation and variance estimation

In the following sections, the modeling steps and the associated variance estimators are described starting from the allometric models. For derivation of the estimators, see Saarela et al. (2023).

A.1. Biomass allometry

The species-specific biomass models by Repola (2008, 2009) were used to predict allometric AGB for each measured tree in the field plots using the calipered DBH and predicted tree height. As the Repola models were fitted using log-transformation, the predicted values were corrected for bias. The predicted individual tree biomass values were then aggregated to produce plot-level AGB density $\widehat{\mathrm{AGBD}}_{\mathrm{plot}}$.

For variance estimation, we need to calculate the covariance matrix of $\widehat{\mathrm{AGBD}}_{\mathrm{plot}}$. Let us first combine the species-specific biomass models into a single model using binary species indicator variables s_{pi}, s_{sp}, and s_{de} for pine, spruce and deciduous trees, respectively:

$$\mathrm{AGB}(\hat{\boldsymbol{\alpha}}, d, h, \mathbf{s}) = s_{\mathrm{pi}}\mathrm{AGB}_{\mathrm{pi}}(\hat{\boldsymbol{\alpha}}_{\mathrm{pi}}, d, h) + s_{\mathrm{sp}}\mathrm{AGB}_{\mathrm{sp}}(\hat{\boldsymbol{\alpha}}_{\mathrm{sp}}, d, h) + s_{\mathrm{de}}\mathrm{AGB}_{\mathrm{de}}(\hat{\boldsymbol{\alpha}}_{\mathrm{de}}, d, h), \quad (A.1)$$

where $\hat{\boldsymbol{\alpha}} = \left[\hat{\boldsymbol{\alpha}}_{\mathrm{pi}}, \hat{\boldsymbol{\alpha}}_{\mathrm{sp}}, \hat{\boldsymbol{\alpha}}_{\mathrm{de}}\right]^T$, in which e.g. $\hat{\boldsymbol{\alpha}}_{\mathrm{pi}}$ is the fitted parameters for the biomass model of pine, d is diameter at breast height, h is tree height, and $\mathbf{s} = \left[s_{\mathrm{pi}}, s_{\mathrm{sp}}, s_{\mathrm{de}}\right]^T$.

We then use Taylor approximation to calculate the covariance matrix of the tree-level AGB predictions:

$$\widehat{\mathbf{C}}_{\text{tree}} = \mathbf{J}_{\text{tree}}^T \widehat{\mathbf{C}}_{\boldsymbol{\alpha}} \mathbf{J}_{\text{tree}}. \tag{A.2}$$

where $\widehat{\mathbf{C}}_{\boldsymbol{\alpha}} = \text{diag}\left(\widehat{\mathbf{C}}_{\boldsymbol{\alpha}_{pi}}, \widehat{\mathbf{C}}_{\boldsymbol{\alpha}_{sp}}, \widehat{\mathbf{C}}_{\boldsymbol{\alpha}_{de}}\right)$ is a block-diagonal matrix consisting of the estimated covariance matrices of the species-specific biomass models reported in Ståhl et al. (2014). The matrix $\mathbf{J}_{\text{tree}}$ is the Jacobian matrix of the combined model (7), which is formed from the partial derivatives

$$\mathbf{J}_{\text{tree}}[i,j] = \frac{\partial \text{AGB}(\hat{\boldsymbol{\alpha}}, d_i, h_i, \mathbf{s}_i)}{\partial \hat{\alpha}_j}, \tag{A.3}$$

where d_i, h_i, and $\mathbf{s}_i$ are the DBH, height and the species of the i'th tree.

To produce $\widehat{\text{AGBD}}_{\text{plot}}$, tree-level AGBs of each plot are aggregated and then divided by the plot area. These can be written as matrix operations and thus the covariance of $\widehat{\text{AGBD}}_{\text{plot}}$ is

$$\widehat{\mathbf{C}}_{\text{plot}} = \mathbf{A}^{-1}\mathbf{U}\widehat{\mathbf{C}}_{\text{tree}}\mathbf{U}^T\mathbf{A}^{-1}, \tag{A.4}$$

where $\mathbf{A}$ is a diagonal matrix, where A_{ii} is the area in hectares of the i'th plot, and U is an aggregation matrix, for which

$$\mathbf{U}_{ij} = \begin{cases} 1, & j\text{'th tree belongs to } i\text{'th plot} \\ 0, & \text{otherwise} \end{cases} \tag{A.5}$$

A.2. Proxy biomass model

The field plot biomass values $\widehat{\mathbf{AGBD}}_{\text{plot}}$ and metrics from ALS and Sentinel-2 were used to fit a quadratic proxy biomass model with four predictor variables:

$$\mathbf{AGBD}_{\text{proxy}} = \left(\beta_0 + \sum_{i=1}^{4} \beta_i \mathbf{x}^{(i)}\right)^2 + \mathbf{e}_f = f(\boldsymbol{\beta}, \mathbf{x}) + \mathbf{e}_f, \tag{A.6}$$

where β_i are the model coefficients, $\mathbf{x}^{(i)}$ the predictors and $\mathbf{e}_f \sim \mathcal{N}\left(0, \boldsymbol{\Sigma}_f\right)$ is an additive error term. As the spatial autocorrelation of $\mathbf{e}_f$ is not modeled in this study, $\boldsymbol{\Sigma}_f$ is a diagonal matrix.

The covariance matrix $\widehat{\mathbf{C}}_{\boldsymbol{\beta}}$ of the model parameters $\boldsymbol{\beta}$ now depends on two sources of uncertainty: 1) the sample used to fit the model (7), and 2) uncertainty of $\widehat{\mathbf{AGBD}}_{\text{plot}}$ used to fit the model (7). Following Saarela et al. (2020), we use the law of total variance and Taylor approximation of the nonlinear model (7) to write:

$$\begin{aligned} \widehat{\mathbf{C}}_{\boldsymbol{\beta}} &= (\mathbf{J}_f^T \widehat{\boldsymbol{\Sigma}}_f^{-1} \mathbf{J}_f)^{-1} \\ &+ (\mathbf{J}_f^T \widehat{\boldsymbol{\Sigma}}_f^{-1} \mathbf{J}_f)^{-1} \mathbf{J}_f^T \widehat{\boldsymbol{\Sigma}}_f^{-1} \widehat{\mathbf{C}}_{\text{plot}} \widehat{\boldsymbol{\Sigma}}_f^{-1} \mathbf{J}_f (\mathbf{J}_f^T \widehat{\boldsymbol{\Sigma}}_f^{-1} \mathbf{J}_f)^{-1}, \end{aligned} \tag{A.7}$$

where $\mathbf{J}_f$ is the Jacobian matrix of the model $f(\boldsymbol{\beta}, \mathbf{x})$ with respect to β, which is formed from the partial derivatives

$$\mathbf{J}_f[i,j] = \frac{\partial f(\beta, \mathbf{x}^{(i)})}{\partial \beta_j}, \tag{A.8}$$

where $\mathbf{x}^{(i)}$ is the predictor vector of the i'th field plot.

The trained proxy AGBD model was then used to predict on the 15 × 15 m subcells of the ICESat −2 segments and the proxy AGBD for the whole 90 m ICESat −2 segment was acquired by averaging the subcell predictions. By using Taylor approximation and writing the subcell averaging as a matrix operator, the covariance for the 90 m proxy AGBD is

$$\widehat{\mathbf{C}}_{\text{proxy}} = \mathbf{M}^T \mathbf{J}_{f*}^T \widehat{\mathbf{C}}_{\boldsymbol{\beta}} \mathbf{J}_{f*} \mathbf{M}, \tag{A.9}$$

where $\mathbf{J}_{f*}$ is the Jacobian matrix of the proxy AGB model evaluated at the 15 m subcell predictor vectors and $\mathbf{M}$ is the averaging matrix, for which

$$\mathbf{M}[i,j] = \begin{cases} \frac{1}{6}, & \text{subcell } i \text{ belongs to segment } j \\ 0, & \text{otherwise.} \end{cases} \tag{A.10}$$

A.3. ICESat −2 biomass model

The ICESat −2 biomass model had the same form as the proxy biomass model (A.6):

$$\mathbf{AGBD}_{\text{I2}} = \left(\gamma_0 + \sum_{i=1}^{4} \gamma_i \mathbf{y}^{(i)}\right)^2 + \mathbf{e}_g = g(\boldsymbol{\gamma}, \mathbf{y}) + \mathbf{e}_g, \tag{A.11}$$

where γ_i are the model coefficients, $\mathbf{y}^{(i)}$ the four ICESat −2 predictors, and $\mathbf{e}_g \sim \mathcal{N}\left(0, \boldsymbol{\Sigma}_g\right)$ is an additive error term. As with the proxy biomass model, spatial autocorrelation of $\mathbf{e}_g$ was not modeled and $\boldsymbol{\Sigma}_g$ is a diagonal matrix.

The covariance matrix of the model coefficients $\boldsymbol{\gamma}$ was calculated in a similar way as previously:

$$\begin{aligned} \widehat{\mathbf{C}}_{\boldsymbol{\gamma}} &= (\mathbf{J}_g^T \widehat{\boldsymbol{\Sigma}}_g^{-1} \mathbf{J}_g)^{-1} \\ &+ (\mathbf{J}_g^T \widehat{\boldsymbol{\Sigma}}_g^{-1} \mathbf{J}_g)^{-1} \mathbf{J}_g^T \widehat{\boldsymbol{\Sigma}}_g^{-1} \widehat{\mathbf{C}}_{\text{proxy}} \widehat{\boldsymbol{\Sigma}}_g^{-1} \mathbf{J}_g (\mathbf{J}_g^T \widehat{\boldsymbol{\Sigma}}_g^{-1} \mathbf{J}_g)^{-1}, \end{aligned} \tag{A.12}$$

where $\mathbf{J}_g$ is the Jacobian matrix of the model $g(\boldsymbol{\gamma}, \mathbf{y})$ with respect to γ evaluated at the Valtimo ICESat −2 segment predictor vectors.

The AGBD values for the Nurmes ICESat −2 segments were then predicted using the fitted ICESat −2 model. The covariance matrix of these predictions is

$$\widehat{\mathbf{C}}_{\text{I2}} = \mathbf{J}_{g*}^T \widehat{\mathbf{C}}_{\boldsymbol{\gamma}} \mathbf{J}_{g*}, \tag{A.13}$$

where $\mathbf{J}_{g*}$ is the Jacobian matrix evaluated at the Nurmes ICESat −2 segment predictor vectors.

A.4. Reference estimate

The reference estimate is a hierarchical model-based estimate following Saarela et al. (2020) using wall-to-wall predicted AGBD from local ALS and Sentinel-2 data in the Nurmes area. The model based on the ALS and Sentinel-2 data had the same form as the Valtimo proxy AGBD model (Appendix A.2). Let us denote the model by $\text{AGBD}, \text{ref} = h(\boldsymbol{\delta}, \mathbf{z}) + \mathbf{e}_{\text{ref}}$. The covariance of the fitted model parameters $\widehat{\mathbf{C}}_{\boldsymbol{\delta}}$ was then estimated similar to Eq. (A.7).

The model based on ALS and Sentinel-2 data was then used to produce a 15 × 15 m wall-to-wall AGBD raster over the Nurmes area. The hierarchical model-based estimate is then the average of the predicted AGBD. The variance of the average AGBD is

$$\widehat{\text{Var}}(\hat{\mu}_{\text{ref}}) = \frac{1}{n_{\text{pix}}^2} \mathbf{1}^T \mathbf{J}_{h*}^T \widehat{\mathbf{C}}_{\delta} \mathbf{J}_{h*} \mathbf{1}, \tag{A.14}$$

where n_{pix} is the total number of forested pixels in the raster.

References

Boudreau, J., Nelson, R.F., Margolis, H.A., Beaudoin, A., Guindon, L., Kimes, D.S., 2008. Regional aboveground forest biomass using airborne and spaceborne LiDAR in Québec. Remote Sens. Environ. 112 (10), 3876–3890.

Breidenbach, J., Granhus, A., Hylen, G., Eriksen, R., Astrup, R., 2020. A century of National Forest Inventory in Norway–informing past, present, and future decisions. For. Ecosyst. 7, 1–19.

Dubayah, R., Armston, J., Healey, S.P., Bruening, J.M., Patterson, P.L., Kellner, J.R., Duncanson, L., Saarela, S., Ståhl, G., Yang, Z., et al., 2022. GEDI launches a new era of biomass inference from space. Environ. Res. Lett. 17 (9), 095001.

Dubayah, R., Blair, J.B., Goetz, S., Fatoyinbo, L., Hansen, M., Healey, S., Hofton, M., Hurtt, G., Kellner, J., Luthcke, S., et al., 2020. The global ecosystem dynamics investigation: High-resolution laser ranging of the Earth's forests and topography. Sci. Remote Sens. 1, 100002.

Duncanson, L., Armston, J., Disney, M., Avitabile, V., Barbier, N., Calders, K., Carter, S., Chave, J., Herold, M., Crowther, T.W., et al., 2019. The importance of consistent global forest aboveground biomass product validation. Surv. Geophys. 40 (4), 979–999.

Duncanson, L., Kellner, J.R., Armston, J., Dubayah, R., Minor, D.M., Hancock, S., Healey, S.P., Patterson, P.L., Saarela, S., Marselis, S., et al., 2022. Aboveground biomass density models for NASA's Global Ecosystem Dynamics Investigation (GEDI) lidar mission. Remote Sens. Environ. 270, 112845.

Eerikäinen, K., 2009. A multivariate linear mixed-effects model for the generalization of sample tree heights and crown ratios in the Finnish National Forest Inventory. For. Sci. 55 (6), 480–493.

Esteban, J., McRoberts, R.E., Fernández-Landa, A., Tomé, J.L., Næsset, E., 2019. Estimating forest volume and biomass and their changes using random forests and remotely sensed data. Remote Sens. 11 (16), 1944.

Finnish Forest Centre, 2021. Forest mask. https://www.metsakeskus.fi/fi/avoin-metsa-ja-luontotieto/aineistot-paikkatieto-ohjelmille/paikkatietoaineistot. (Accessed 23 February 2022) (in Finnish).

Fortin, M., van Lier, O., Côté, J.F., 2022. Combining forest growth models and remotely sensed data through a hierarchical model-based inferential framework. Can. J. Forest Res.

Gregoire, T.G., Valentine, H.T., 2007. Sampling Strategies for Natural Resources and the Environment. CRC Press.

Guerra-Hernández, J., Narine, L.L., Pascual, A., Gonzalez-Ferreiro, E., Botequim, B., Malambo, L., Neuenschwander, A., Popescu, S.C., Godinho, S., 2022. Above-ground biomass mapping by integrating ICESat-2, SENTINEL-1, SENTINEL-2, ALOS2/PALSAR2, and topographic information in mediterranean forests. GISci. Remote Sens. 59 (1), 1509–1533.

Healey, S.P., Patterson, P.L., Saatchi, S., Lefsky, M.A., Lister, A.J., Freeman, E.A., 2012. A sample design for globally consistent biomass estimation using lidar data from the Geoscience Laser Altimeter System (GLAS). Carbon Balanc. Manag. 7 (1), 1–9.

Holm, S., Nelson, R., Ståhl, G., 2017. Hybrid three-phase estimators for large-area forest inventory using ground plots, airborne lidar, and space lidar. Remote Sens. Environ. 197, 85–97.

Isenburg, M., 2020. LAStools - efficient tools for LiDAR processing. version 201003, http://lastools.org.

Lefsky, M.A., Harding, D.J., Keller, M., Cohen, W.B., Carabajal, C.C., Del Bom Espirito-Santo, F., Hunter, M.O., de Oliveira, Jr., R., 2005. Estimates of forest canopy height and aboveground biomass using ICESat. Geophys. Res. Lett. 32 (22).

Main-Knorn, M., Pflug, B., Louis, J., Debaecker, V., Müller-Wilm, U., Gascon, F., 2017. Sen2Cor for Sentinel-2. In: Image and Signal Processing for Remote Sensing XXIII, Vol. 10427. International Society for Optics and Photonics, 1042704.

Maltamo, M., Eerikäinen, K., Packalén, P., Hyyppä, J., 2006. Estimation of stem volume using laser scanning-based canopy height metrics. Forestry 79 (2), 217–229.

Margolis, H.A., Nelson, R.F., Montesano, P.M., Beaudoin, A., Sun, G., Andersen, H.E., Wulder, M.A., 2015. Combining satellite lidar, airborne lidar, and ground plots to estimate the amount and distribution of aboveground biomass in the boreal forest of North America. Can. J. Forest Res. 45 (7), 838–855.

Markus, T., Neumann, T., Martino, A., Abdalati, W., Brunt, K., Csatho, B., Farrell, S., Fricker, H., Gardner, A., Harding, D., et al., 2017. The Ice, Cloud, and land Elevation Satellite-2 (ICESat-2): science requirements, concept, and implementation. Remote Sens. Environ. 190, 260–273.

Narine, L.L., Popescu, S.C., Malambo, L., 2020. Using ICESat-2 to estimate and map forest aboveground biomass: A first example. Remote Sens. 12 (11), 1824.

Narine, L.L., Popescu, S., Neuenschwander, A., Zhou, T., Srinivasan, S., Harbeck, K., 2019. Estimating aboveground biomass and forest canopy cover with simulated icesat-2 data. Remote Sens. Environ. 224, 1–11.

Neigh, C.S., Nelson, R.F., Ranson, K.J., Margolis, H.A., Montesano, P.M., Sun, G., Kharuk, V., Næsset, E., Wulder, M.A., Andersen, H.E., 2013. Taking stock of circumboreal forest carbon with ground measurements, airborne and spaceborne LiDAR. Remote Sens. Environ. 137, 274–287.

Nelson, R., Boudreau, J., Gregoire, T.G., Margolis, H., Næsset, E., Gobakken, T., Ståhl, G., 2009. Estimating Quebec provincial forest resources using ICESat/GLAS. Can. J. Forest Res. 39 (4), 862–881.

Nelson, R., Margolis, H., Montesano, P., Sun, G., Cook, B., Corp, L., Andersen, H.E., de-Jong, B., Pellat, F.P., Fickel, T., et al., 2017. Lidar-based estimates of aboveground biomass in the continental US and Mexico using ground, airborne, and satellite observations. Remote Sens. Environ. 188, 127–140.

Neuenschwander, A., Pitts, K., Jelley, B., Robbins, J., Klotz, B., Popescu, S., Nelson, R., Harding, D., Pederson, D., Sheridan, R., 2021. ATLAS/ICESat-2 L3A Land and Vegetation Height, Version 4. NASA National Snow and Ice Data Center Distributed Active Archive Center, Boulder, Colorado USA, http://dx.doi.org/10.5067/ATLAS/ATL08.004 (Accessed 19 April 2021).

Neumann, T., Brenner, A., Hancock, D., Robbins, J., Saba, J., Harbeck, K., Gibbons, A., Lee, J., Luthcke, S., Rebold, T., et al., 2021. ATLAS/ICESat-2 L2A Global Geolocated Photon Data, Version 4. NASA National Snow and Ice Data Center Distributed Active Archive Center, Boulder, Colorado USA, http://dx.doi.org/10.5067/ATLAS/ATL03.004 (Accessed 19 April 2021).

Neumann, T.A., Martino, A.J., Markus, T., Bae, S., Bock, M.R., Brenner, A.C., Brunt, K.M., Cavanaugh, J., Fernandes, S.T., Hancock, D.W., et al., 2019. The Ice, Cloud, and Land Elevation Satellite–2 Mission: A global geolocated photon product derived from the advanced topographic laser altimeter system. Remote Sens. Environ. 233, 111325.

Packalen, P., Strunk, J., Packalen, T., Maltamo, M., Mehtätalo, L., 2019. Resolution dependence in an area-based approach to forest inventory with airborne laser scanning. Remote Sens. Environ. 224, 192–201.

Packalen, P., Temesgen, H., Maltamo, M., 2012. Variable selection strategies for nearest neighbor imputation methods used in remote sensing based forest inventory. Can. J. Remote Sens. 38 (5), 557–569. http://dx.doi.org/10.5589/m12-046.

Patterson, P.L., Healey, S.P., Ståhl, G., Saarela, S., Holm, S., Andersen, H.E., Dubayah, R.O., Duncanson, L., Hancock, S., Armston, J., et al., 2019. Statistical properties of hybrid estimators proposed for GEDI – NASA's global ecosystem dynamics investigation. Environ. Res. Lett. 14 (6), 065007.

Pinheiro, J., Bates, D., R. Core Team, 2021. nlme: Linear and nonlinear mixed effects models. URL: https://CRAN.R-project.org/package=nlme, R package version 3.1-152.

Repola, J., 2008. Biomass equations for birch in Finland. Silva Fennica 42 (4), 605–624.

Repola, J., 2009. Biomass equations for Scots pine and Norway spruce in Finland. Silva Fennica 43 (4), 625–647.

Saarela, S., Holm, S., Grafström, A., Schnell, S., Næsset, E., Gregoire, T.G., Nelson, R.F., Ståhl, G., 2016. Hierarchical model-based inference for forest inventory utilizing three sources of information. Ann. For. Sci. 73 (4), 895–910.

Saarela, S., Holm, S., Healey, S.P., Andersen, H.E., Petersson, H., Prentius, W., Patterson, P.L., Næsset, E., Gregoire, T.G., Ståhl, G., 2018. Generalized hierarchical model-based estimation for aboveground biomass assessment using GEDI and Landsat data. Remote Sens. 10 (11), 1832.

Saarela, S., Holm, S., Healey, S.P., Patterson, P.L., Yang, Z., Andersen, H.E., Dubayah, R.O., Qi, W., Duncanson, L.I., Armston, J.D., et al., 2022. Comparing frameworks for biomass prediction for the Global Ecosystem Dynamics Investigation. Remote Sens. Environ. 278, 113074.

Saarela, S., Varvia, P., Korhonen, L., Yang, Z., Patterson, P.L., Gobakken, T., Næsset, E., Healey, S.P., Ståhl, G., 2023. Three-phase hierarchical model-based and hybrid inference. MethodsX 11, 102321.

Saarela, S., Wästlund, A., Holmström, E., Mensah, A.A., Holm, S., Nilsson, M., Fridman, J., Ståhl, G., 2020. Mapping aboveground biomass and its prediction uncertainty using LiDAR and field data, accounting for tree-level allometric and LiDAR model errors. For. Ecosyst. 7, 1–17.

Song, H., Xi, L., Shu, Q., Wei, Z., Qiu, S., 2022. Estimate forest aboveground biomass of mountain by ICESat-2/ATLAS data interacting cokriging. Forests 14 (1), 13.

Ståhl, G., Heikkinen, J., Petersson, H., Repola, J., Holm, S., 2014. Sample-based estimation of greenhouse gas emissions from forests—a new approach to account for both sampling and model errors. For. Sci. 60 (1), 3–13.

Ståhl, G., Holm, S., Gregoire, T.G., Gobakken, T., Næsset, E., Nelson, R., 2011. Model-based inference for biomass estimation in a LiDAR sample survey in Hedmark County, Norway. Can. J. Forest Res. 41 (1), 96–107.

Varvia, P., Korhonen, L., Bruguière, A., Toivonen, J., Packalen, P., Maltamo, M., Saarela, S., Popescu, S.C., 2022. How to consider the effects of time of day, beam strength, and snow cover in ICESat-2 based estimation of boreal forest biomass? Remote Sens. Environ. 280, 113174.

Wilkes, P., Jones, S.D., Suarez, L., Haywood, A., Woodgate, W., Soto-Berelov, M., Mellor, A., Skidmore, A.K., 2015. Understanding the effects of ALS pulse density for metric retrieval across diverse forest types. Photogramm. Eng. Remote Sens. 81 (8), 625–635.

Wulder, M.A., White, J.C., Bater, C.W., Coops, N.C., Hopkinson, C., Chen, G., 2012. Lidar plots—A new large-area data collection option: Context, concepts, and case study. Can. J. Remote Sens. 38 (5), 600–618.